CHAPTER 10

EPR INVESTIGATION OF [NIFE] HYDROGENASES

Maurice van Gastel and Wolfgang Lubitz

Max-Planck-Institut für Bioanorganische Chemie, Mülheim an der Ruhr, Germany

EPR studies of the [NiFe] hydrogenases are reviewed. These enzymes contain a heterobimetallic [NiFe] center as the active site. The nickel is ligated to four cysteine residues, two of which form a bridge to the iron. The iron carries additionally 3 small inorganic diatomic ligands ($2CN^-$, CO). A third small ligand X is situated in the bridge between Ni and Fe. In the catalytic cycle the enzyme passes through a number of redox states, several of which are paramagnetic. The iron remains in the divalent low-spin (Fe^{II}, S = 0) state, whereas the nickel changes its valence and spin state during this cycle. Nickel is believed to bind the hydrogen and to be directly involved in the catalytic process. The available EPR data are interpreted in terms of a simple model, based on ligand field theory. The model indicates that the paramagnetic Ni–A, Ni–B, and Ni–C states are best described as formal Ni^{III} low-spin species with a spin of $S = 1/2$ and a d_{z^2} ground state. The d_{z^2} orbital is oriented along the molecular z axis (g_z axis, $g_z \approx g_e$) and points to the open coordination site of the Ni. The "EPR-silent" states are all Ni^{II} species. XAS spectroscopy provides evidence that these states are high-spin ($S = 1$) states; however, supporting EPR spectra have not yet been reported. The light-induced Ni–L states are characterized by a nickel d_{z^2} ground state with an admixture of the $d_{x^2-y^2}$ orbital. The identity of the third bridging ligand X between nickel and iron changes upon going from Ni–A to Ni–B to Ni–C and to Ni–L. ENDOR and HYSCORE data indicate that a μ-OH^- bridge is present in Ni–B, for Ni–C a formal μ-H^- has been identified, while for Ni–L the bridge is empty. The bridging ligand of the Ni–A state is still under debate. The identification of the electronic and geometric structure of the reaction intermediates employing spectroscopy and quantum chemical calculations form the basis for setting up a reaction mechanism for the [NiFe] hydrogenase.

G. Hanson, L. Berliner (eds.), *High Resolution EPR*, Biological Magnetic Resonance 28,
DOI 10.1007/978-0-387-84856-3_10, © Springer Science+Business Media, LLC 2009

1. CLASSIFICATION, COMPOSITION AND STRUCTURE OF HYDROGENASES

Hydrogenases catalyze the reversible heterolytic splitting of molecular hydrogen:

$$H_2 \rightleftharpoons H^- + H^+ \rightleftharpoons 2\,H^+ + 2\,e^- \quad (1)$$

These enzymes are found in many archae, bacteria, and even a few eukaryotes [1]. One of the most common groups are the sulfate-reducing bacteria of the *Desulfovibrio* (*D.*) species. Because of their ability not only to utilize hydrogen as an energy source but also to produce molecular hydrogen from protons, they have been the subject of many investigations with the aim to better understand the catalytic activity. Hydrogenases are commonly divided into classes according to the metal content of the active site, where the catalytic activity takes place. Presently, three classes of hydrogenases have been identified: the [Fe], the [FeFe], and the [NiFe] hydrogenases [1]. For the [NiFe] hydrogenases, x-ray structures exist for the enzymes of the organisms of *D. gigas* [2–5], *D. vulgaris* Miyazaki F [6–9], *D. fructosovorans* [5,10], *D. baculatum* [4], and *D. desulfuricans* [11]. Other [NiFe] hydrogenases that have been extensively studied are from *Allochromatium* (*A.*) *vinosum* [12–20] and *Ralstonia (R.) eutropha* [21–28]. In *R. eutropha* a membrane-bound standard hydrogenase, a soluble (NADP-reducing) hydrogenase and a regulatory hydrogenase (RH) have been found. The latter (RH) acts as a hydrogen sensor and has an active site similar to the catalytic hydrogenase [29].

The [NiFe] hydrogenases consist of two subunits with molecular weights of about 30 and 60 kDa (Fig. 1). For the membrane-bound enzymes a small membrane anchor is present as well, which is cleaved during the purification process. The large subunit contains the active site. The geometry of the active site is highly conserved throughout all [NiFe] hydrogenases (Fig. 1). The nickel and iron atoms are separated by a distance of about 2.5 to 2.9 Å and are bridged by the sulfur atoms of two cysteines. The nickel is coordinated by two more cysteines bound in a terminal position. For some hydrogenases one of the latter cysteines is replaced by a selenocysteine, and these enzymes form the subclass of [NiFeSe] hydrogenases. The iron atom carries three inorganic diatomic ligands that have been identified by infrared spectroscopy as two CN^- and one CO [30]. In the oxidized state (in general a mixture of the so-called "unready" Ni–A and the "ready" Ni–B states), additional density is visible between nickel and iron that stems from a third bridging ligand "X" [3,6]. In the reduced Ni–C state this density is absent [4,7]. However, from the x-ray data it cannot be concluded if position X is empty or occupied by an atom or molecule with low electron density. Recent spectroscopic results will be discussed that point to the presence of a bridging hydride H^- in this state.

The small subunit contains three [FeS] clusters that are involved in the electron transport to/from the active [NiFe] center (Fig. 1). In the catalytically active hydrogenases, a [4Fe4S] "proximal" cluster is located near the [NiFe] center,

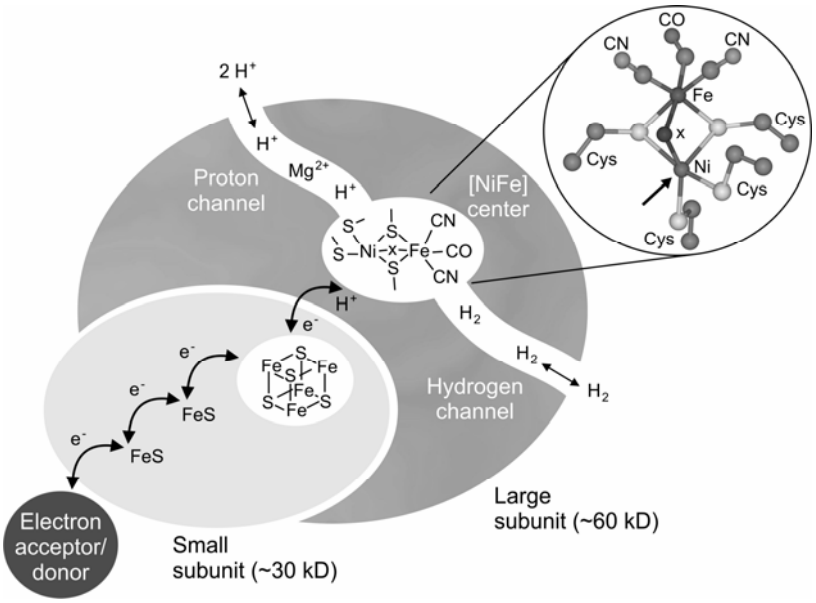

Figure 1. Schematic view of an [NiFe] hydrogenase and the active site. Shown are the 2 subunits with the active site (NiFe center), the proton channel, and the hydrogen access channel in the large subunit and the electron transport chain (3 FeS centers) in the small subunit. The structure of the catalytic site is shown on the right, which is based on the x-ray crystallographic analysis of *D. vulgaris* Miyazaki F [6]. Note that Fe is six-coordinate, while Ni is only five-coordinate; the free coordination site at Ni is marked by an arrow. For further details see text.

flanked by a [3Fe4S] cluster. Near the protein surface another [4Fe4S] "distal" cluster is present. Also indicated in Figure 1 is a magnesium ion found in the crystal structure, which is probably located in the proton transfer channel. A possible pathway for molecular hydrogen to travel between the protein surface and the active site has been found in crystallographic studies using high-pressure Xe gas [31,32].

The [NiFe] center is rich in redox states. The oxidized states (Ni–A, Ni–B) are catalytically inactive and can be activated by reduction with molecular hydrogen. They differ in their activation kinetics: Ni–A takes hours to be activated under hydrogen, while Ni–B takes only minutes [33]. For this reason the Ni–A state is also called the "unready" state and the Ni–B state the "ready" state. Both states are paramagnetic and are characterized by different *g*-values (Table 1). Upon one-electron reduction of Ni–A and Ni–B, the EPR-silent states Ni–SU and Ni–SIr are formed. For *A. vinosum* hydrogenase it has been shown that the Ni–A $\rightarrow$ Ni–SU reduction is reversible, but the Ni–B $\rightarrow$ Ni–SIr reduction strongly depends on pH and temperature. At pH 6.0 and 2ºC the reduction was completely irreversible, at pH 8 and 30ºC both reductions were reversible [16]. For *A. vinosum* hydrogenase

Table 1. Summary of *g* Values of the EPR Active States in Standard [NiFe] Hydrogenases

	g_x (g_1)	g_y (g_2)	g_z (g_3)
Ni–A	2.32	2.24	2.01
Ni–B	2.33	2.16	2.01
Ni–C	2.20	2.15	2.01
Ni–L1	2.30	2.12	2.05
Ni–L2	2.26	2.11	2.05
Ni–L3	2.41	2.16	n.d.
Ni–CO	2.12	2.07	2.02

All values taken from *D. vulgaris* Miyazaki F [51] except for Ni–CO (*A. vinosum*) [36] and Ni–L3 (*D. gigas*) [35]. For the orientation of axes see Figure 7. n.d. = not determined.

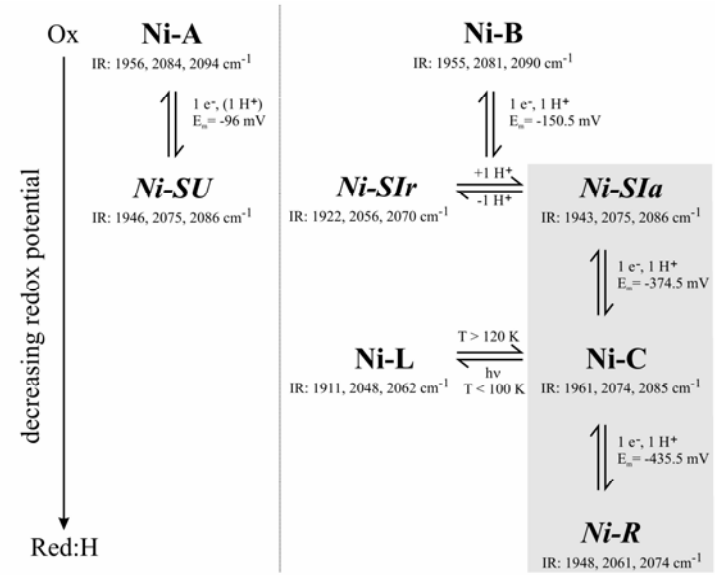

Figure 2. Overview of the redox states of [NiFe] hydrogenases, from the most oxidized (top) to the most reduced (bottom) form. Indicated are the IR frequencies (IR) of the CO ligand and the two CN^- ligands to Fe for *D. vulgaris* Miyazaki F hydrogenase and the midpoint potentials (E_m) for the redox transitions at pH = 6 (Ni–A/*NiSU*) and at pH = 7.4 (all others). The paramagnetic states are given in bold face, the EPR-silent states in italics. The two states *Ni–SIr* and *Ni–SIa* are in an acid–base equilibrium. The states involved directly in the catalytic cycle are highlighted by a shaded box. The paramagnetic Ni–CO state (not shown) is probably derived from the Ni–L state.

under reducing conditions and at temperatures greater than or equal to 30ºC, the Ni–SIr is converted into another EPR-silent state, Ni–SIa, which can be quickly reduced to give another EPR active state Ni–C [15]. The Ni–C state exhibits a characteristic rhombic **g** tensor, and this state is found in all enzymes studied so far

(Table 1). The Ni–C state is light sensitive. Upon illumination with white light, the characteristic EPR signal disappears and a new signal appears [34], which is called Ni–L. At least two subforms have been identified with different *g* values, Ni–L1 and Ni–L2, depending on the temperature and the duration of light exposure [35]. Upon further reduction in the presence of H_2, the most reduced state, Ni–R, is formed. Ni–R is EPR silent. Three subforms of Ni–R have been identified for *A. vinosum* hydrogenase [14]; however, the presence of all these substates has not yet been experimentally confirmed in hydrogenases from other sources. The [NiFe] hydrogenase can be inhibited by the addition of CO. It has been shown by x-ray crystallography of single crystals treated with CO [8] that the CO binds at the sixth free coordination site of the nickel (see Fig. 1). A paramagnetic Ni–CO state has been described and characterized [19,34,36,37]. This Ni–CO is also photosensitive, and upon illumination at low temperatures, CO photodissociates, resulting in the same Ni–L state as Ni–C. The different EPR active and EPR-silent redox states of the [NiFe] hydrogenase are depicted in the scheme shown in Figure 2.

In this contribution, an overview is given of the EPR studies performed so far on the EPR active states Ni–A, Ni–B, Ni–C, Ni–L, and Ni–CO. The emphasis here lies on the identification of the structure of the active site in all these intermediate states, including the assignment of the bridging ligand "X." Knowledge of the exact structures of all intermediates is an essential prerequisite for quantum chemical studies, from which a reaction mechanism can be proposed. Especially, advanced EPR methods like ENDOR, ESEEM, and HYSCORE have played a crucial role in determining the hyperfine coupling constants (HFCs) of the metal nuclei and identifying protons or nitrogens from nearby amino acids or non-protein ligands, and in this way have helped to characterize both the electronic and the geometric structure of the site. The EPR-silent states have been investigated by other spectroscopic methods like XAS [38–41] and FTIR spectroscopy [14,42,43].

2. BASIC DESCRIPTION OF THE ELECTRONIC STRUCTURE

Many of the spectroscopic observables, especially those related to EPR spectroscopy, can be rationalized, when considering the crystal field of the metal ions. The x-ray structure shows [5,9] that the iron is hexacoordinate in all states. ENDOR data (*vide infra*) indicate that this atom remains in the non-paramagnetic ($S = 0$) low-spin Fe^{II} state in all EPR active redox states. This is probably caused by the tightly bound CO and CN^- ligands. The nickel ion is coordinated by five ligands in the Ni–A and Ni–B states [2], four of which (three sulfurs of cysteines and the bridging ligand "X") form the base plane of a square pyramid. The fifth ligand (the sulfur of the fourth cysteine) occupies an axial position, and the other axial ligation position is unoccupied (see Fig. 1). The square pyramidal crystal field gives rise to a characteristic energy splitting of the five 3d orbitals at nickel.

The effect of the ligand field on a five-coordinate metal has been described by Solomon et al. [44]. The results presented in [44] were obtained for an Fe^{II} with four equatorial oxygen ligands and a unique axial ligand. The symmetry of this crystal field also applies to a five-coordinate nickel. A schematic overview of a

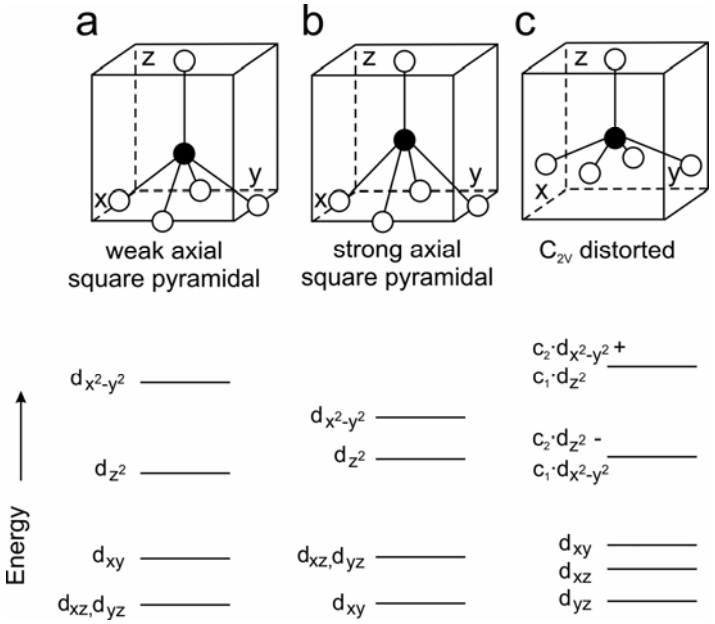

Figure 3. Schematic representation of the ligand field splitting of the 3d orbitals of a five-coordinate transition metal. The diagrams are reproduced and modified from [44]. Shown are a square pyramidal ligand field with a weak axial ligand (a); a strong axial ligand (b); C_{2v} distortion (c). In (c) a mixture of d_{z^2} and $d_{x^2-y^2}$ occurs ($c_1^2 + c_2^2 = 1$).

square pyramidal crystal field environment with a weak axial ligand, in which the metal is only slightly lifted out of the equatorial plane, gives rise to a splitting of the d orbitals, as indicated in Figure 3a. The d orbitals of lowest energy are the degenerate d_{xz} and d_{yz} orbitals. For a formal Ni^{III} ion, seven electrons are present in the 3d shell. For this d^7 case the d_{xz}, d_{yz} and d_{xy} orbitals are doubly occupied, and the unpaired electron resides in the d_{z^2} orbital, with the *z* axis defined as being parallel to the axis that connects the nickel and the atom of the axially coordinated ligand.

In this ligand field, the **g**-tensor is characterized by one small principal *g*-value ($g_z \sim g_e$) and two larger *g*-values g_i ($i = x, y$). The **g** tensor components of the d_{z^2} state can be expressed in terms of the spin-orbit-coupling parameter λ at Ni (note that $\lambda_{Ni} < 0$ [45]), and the energies of the d orbitals:

$$g_x = g_e - \frac{6\lambda}{E_{z^2} - E_{yz}} \quad , \quad g_y = g_e - \frac{6\lambda}{E_{z^2} - E_{xz}} \quad , \quad g_z = g_e \cdot \tag{2}$$

The g_x and g_y values are degenerate (axial symmetry) in a ligand field with C_{4v} symmetry but are expected to become unequal in the [NiFe] hydrogenase, due to the asymmetric protein environment. A rhombic **g** tensor is observed for all hydrogenases.

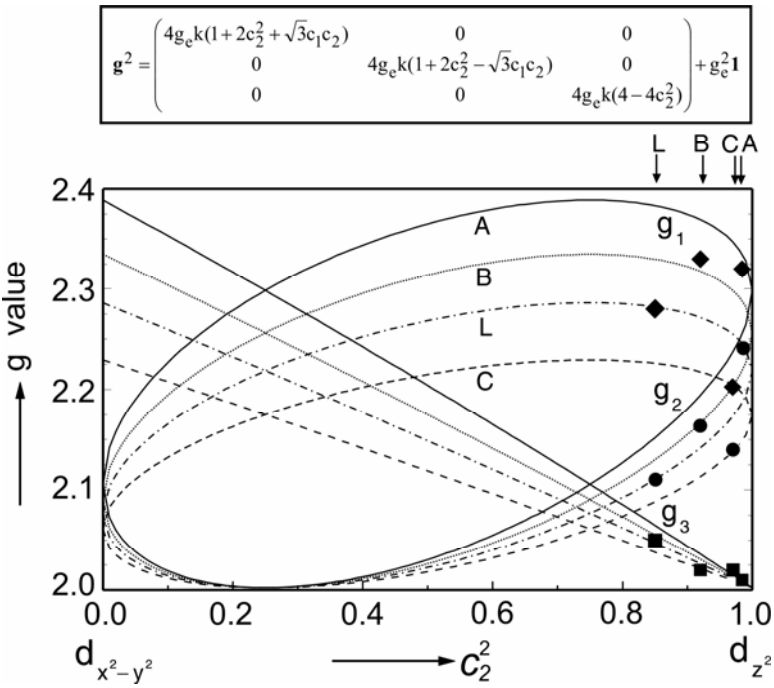

Figure 4. The **g**-tensor components of Ni–A, Ni–B, Ni–C, and Ni–L as a function of d orbital mixing (d_{z^2} and $d_{x^2-y^2}$) for four cases with different perturbation parameters $k = \lambda_{Ni}/\Delta E_{dd}$, which were chosen to be: k(Ni–A) = 0.053 (solid line), k(Ni–B) = 0.045 (dotted line), k(Ni–C) = 0.030 (dashed line), and k(Ni–L) = 0.038 (dashed/dotted line). The experimental values of the four states are indicated by ♦ (g_1), • (g_2), and ■ (g_3). In the model the Ni character of the singly occupied molecular orbital is described by $\Psi_{Ni} = c_1 d_{x^2-y^2} + c_2 d_{z^2}$, the energy of the other molecular orbitals with Ni(3d) character being lower by ΔE_{dd}. The expression derived for the **g** tensor is given at the top of the figure. For further details, see [46].

We now briefly summarize the effect of distortions to the ligand field [44] that are relevant for [NiFe] hydrogenases. When the axial ligand is strongly coordinated, the d_{xy} orbital becomes lowest in energy and the energy of the d_{z^2} orbital approaches that of the $d_{x^2-y^2}$ orbital (the z direction is along the four-fold symmetry axis of the system) (see Fig. 3b). A distortion along one of the two equatorial axes causes a slight mixing of the $d_{x^2-y^2}$ and d_{z^2} orbitals (indicated in Fig. 3c). The effect of such a distortion on the g values has been discussed previously [46], where it was shown that a small admixture of $d_{x^2-y^2}$ orbital causes an increase of the g_z value and an increase in rhombicity without significantly changing the orientation of the g_z axis of the **g** tensor (see Fig. 4).

The above-described ligand field also holds for the Ni^{II} (d^8) and Ni^{I} (d^9) valence states. Ni^{I} is paramagnetic (S = 1/2), and has a $d_{x^2-y^2}$ ground state, for which the **g** tensor components are

$$g_x = g_e - \frac{2\lambda}{E_{xy} - E_{xz}}, \quad g_y = g_e - \frac{2\lambda}{E_{xy} - E_{yz}}, \quad g_z = g_e - \frac{8\lambda}{E_{xy} - E_{x^2-y^2}}. \qquad (3)$$

In this case the *z* principal axis is associated with the largest *g* value, whereas for a d_{z^2} ground state the principal *z* axis is associated with the smallest *g* value. For Ni^{II} the low-spin form is diamagnetic, and the high-spin state has $S = 1$. In case of the Ni–L state, in which one equatorial ligand is removed (*vide infra*), the $d_{x^2-y^2}$ and d_{z^2} orbitals come very close in energy and orbital mixing and the order of the two orbitals may change.

Although a description in terms of pure d orbitals gives insight into the electronic structure, the binding of polarizable ("soft") ligands (cysteine sulfurs) may lead to a significant spin delocalization, leaving only a fraction of the spin at the metal. This delocalization also has consequences for the hyperfine coupling constants (HFCs) of magnetic nuclei near the [NiFe] center. Particularly large HFCs (^{33}S, ^{1}H) are expected for the cysteine residue bound in the axial position along the symmetry axis of the spin carrying d_{z^2} orbital (see Fig. 1).

3. EPR CHARACTERIZATION OF [NiFe] HYDROGENASES: THE G TENSORS

In this section the EPR spectra of the EPR active redox states are discussed. An overview of the spectra for *D. vulgaris* Miyazaki F is given in Figure 5, and a summary of *g* values can be found in Table 1.

3.1. The Oxidized States Ni–A and Ni–B

The first EPR spectrum of the Ni–A state was reported in 1982 [47] for the enzyme of *D. gigas*. In this work, the Ni–B state was also observed and appeared as a minority species. In other species like *D. vulgaris* Miyazaki F [48], the two states exist as mixtures with a more equal ratio in the aerobic "as-isolated" form of the enzyme. Different methods of preparation have been used to separate the Ni–A and Ni–B redox states, such that they appear as pure redox states in the EPR spectrum and can be therefore studied individually [13]. The Ni–A and Ni–B states have the same oxidation level, yet they differ in their *g* values, as observed by EPR (see Fig. 5 and Table 1). The activation times are different [33] and the FTIR spectra show differences with respect to the stretching frequencies of the CN^- and CO ligands attached to iron [14]. The midpoint potential for the Ni–A/Ni–SU couple in *D. gigas* hydrogenase has been investigated by EPR and redox titrations [49], and was found to depend on pH. By using electrochemistry combined with FTIR spectroscopy, the midpoint potentials of other redox states, including Ni–B, have also been investigated [42]. Both states are inactive and do not take part in the catalytic cycle. However, in order to understand the activation (deactivation) of the enzyme

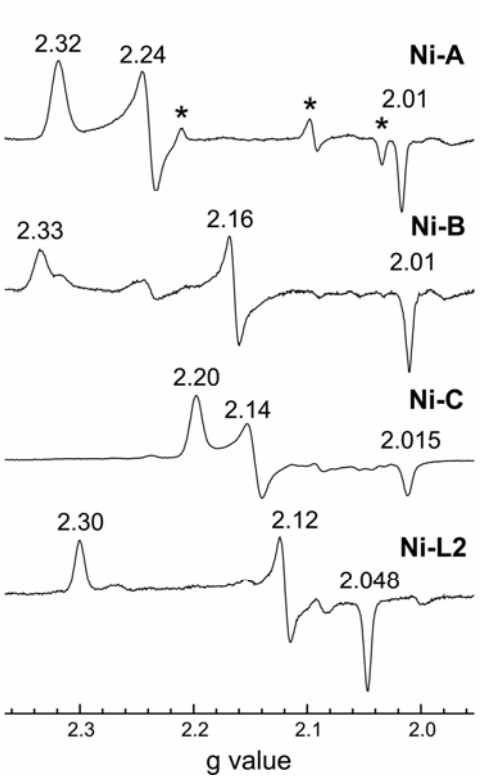

Figure 5. Overview of the EPR spectra of a standard [NiFe] hydrogenase. The spectra were obtained from *D. vulgaris* Miyazaki F in the Ni–A, Ni–B, Ni–C, and Ni–L2 redox states (see text for details). In the spectrum of Ni–A, lines from an additional redox state are observed that are marked with an asterisk. Experimental conditions: ν_{mw} = 9.43 GHz, mod. freq. = 100 kHz, mod. depth = 5 G, recording time for each spectrum = approx. 15 min. For details, see [58].

and the aerobic inhibition, the spectroscopic and chemical differences of the Ni–A and Ni–B states have been the topic of many recent investigations that aim to elucidate the origin of these differences.

Until the mid-1990s, all EPR investigations of hydrogenases have been performed on frozen solutions and the *g* values have mainly been used as "fingerprints" for the identification of redox states (Table 1). With the advent of [NiFe] hydrogenase crystals of sufficient size, the first single-crystal EPR studies became possible and were performed on the enzyme from *D. vulgaris* Miyazaki F [48,50,51]. This opened the possibility to determine, in addition to the **g** tensor principal values, also the tensor axes and their orientations in the molecular frame. With this information the *g* values could be assigned to the geometrical structure

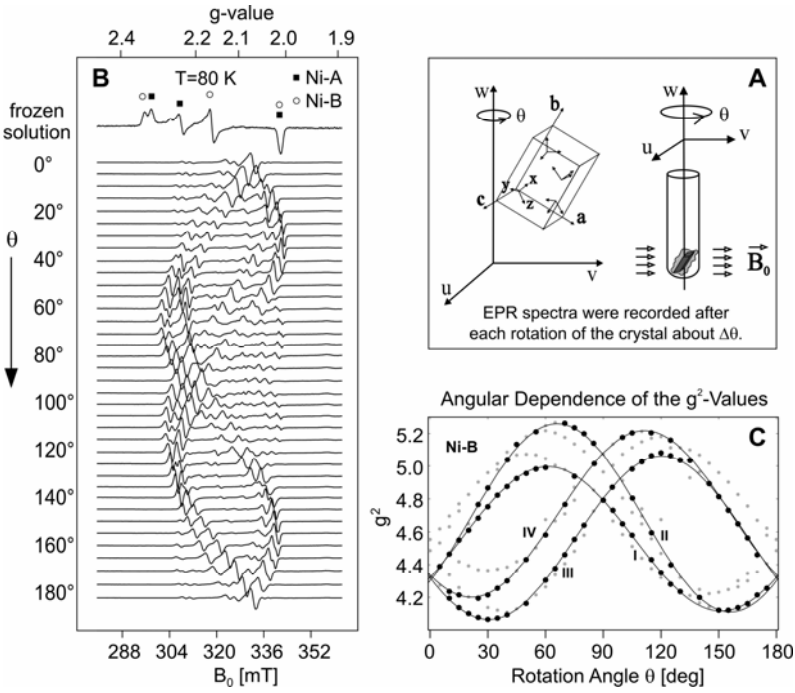

Figure 6. Schematic overview of single-crystal EPR experiments. EPR spectra are taken for different orientations of the crystal with respect to the magnetic field. The orientational dependence of the resonances can be analyzed to elucidate the directions of the principal axes of the **g** tensor with respect to the crystallographic axes. When the crystal structure is known, the information can be combined to obtain the directions of the principal axes with respect to bond directions and the geometry of the active site. The data shown are taken for the Ni–A and Ni–B redox states of *D. vulgaris* Miyazaki F hydrogenase. For details, see [48,50]. (**A**) Single crystal mounted in an EPR sample tube; shown are the laboratory reference frame (u, v, w), the crystal axes (a, b, c) of the orthorhombic single crystal with four sites in the unit cell (space group $P2_12_12_1$), and the molecular/**g** tensor axes (x, y, z). (**B**) *Top*: Frozen solution EPR spectrum (X-band) of an "as-isolated" [NiFe] hydrogenase sample containing Ni–A: Ni–B ~ 2:3. *Bottom*: Angular variation of the EPR spectra of a single crystal (T = 10 K) in an arbitrary orientation showing lines from both Ni–A and Ni–B (and some smaller disoriented crystallites). Note that a maximum of 4 lines (4 sites) is expected for each species. (**C**) Angular dependence of the $\mathbf{g}^2$ tensors of Ni–A (grey) and Ni–B (black). The analysis yields the **g** tensor principal values and the **g** tensor axes in the crystallographic axes system that can be converted to the molecular axes via the known crystallographic structure.

and be related to the d orbitals of the metal. Furthermore, single-crystal EPR experiments can be performed over a wide range of temperatures (from ambient to liquid helium), which allows to follow the structural changes of the enzyme [50]. A schematic overview of the single-crystal experiments performed on Ni–A and Ni–B for *D. vulgaris* Miyazaki F [50] is given in Figure 6. An additional stereoview of the principal axes of the **g** tensor in the Ni–A and Ni–B states is depicted in Figure 7. It was found that the principal g_z axis, corresponding to the smallest g value

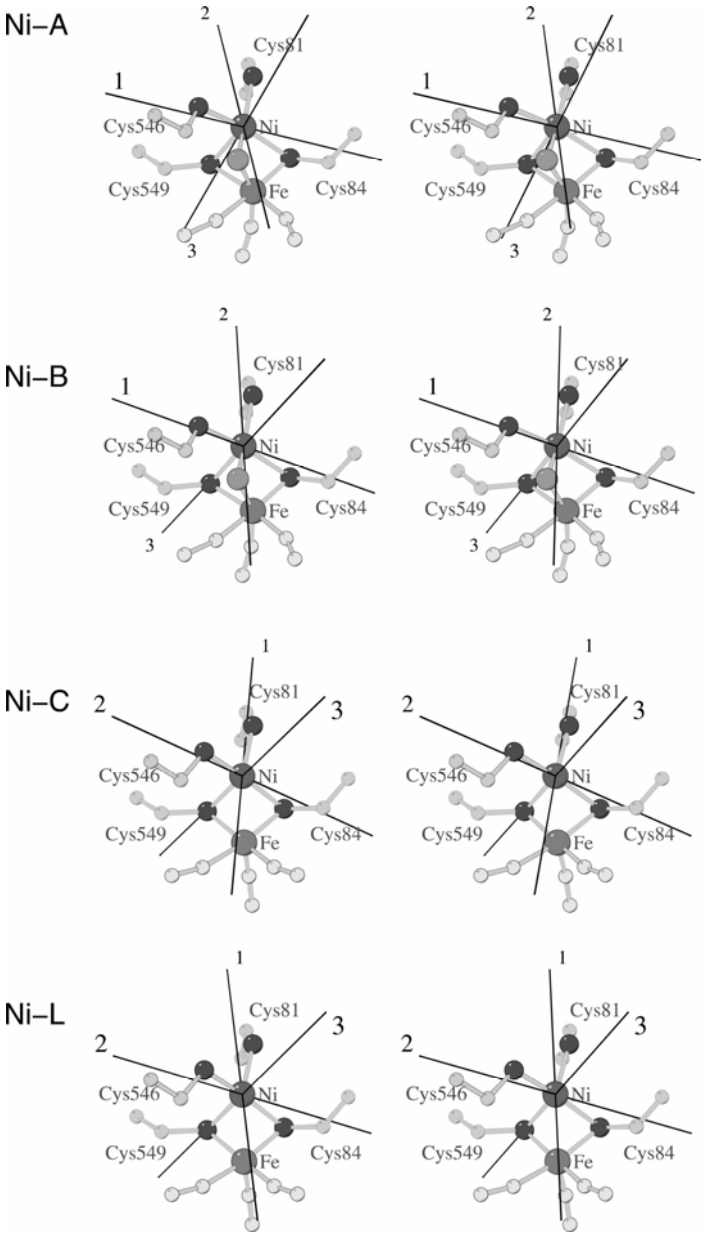

Figure 7. Stereoviews of the directions of the principal axes of the **g** tensors with respect to the geometry of the active site in the Ni–A, Ni–B, Ni–C, and Ni–L2 redox states of [NiFe] hydrogenase from *D. vulgaris* Miyazaki F. Reproduced with permission from [51]. Copyright © 2003, American Chemical Society.

(2.01), is approximately parallel to the bond direction of nickel toward the sulfur of the axial cysteine. This defines the direction of the C_∞ symmetry axis of the $3d_{z^2}$ orbital, which contains the bulk spin density. The g_z axis also points from nickel toward the free coordination position of the square pyramid. This is compatible with a nickel that is either in a square pyramidal or in an octahedral ligand field with a weak axial ligation in both Ni–A and Ni–B forms. The temperature dependence of the EPR spectra between 295 and 10 K exhibited no structural changes of the active site. This is of general importance for the investigation of this enzyme, since it shows that the same *g* values are obtained both under physiological conditions at ambient temperature as well as at cryogenic temperatures. It should also be noted that the principal **g** tensor values are the same within experimental error in frozen solution and in single crystals. Thus, crystallization does not change the electronic structure of the active site.

3.2. The Reduced Active State Ni–C

The Ni–C intermediate state is the only EPR active state that takes part in the catalytic cycle. It is two electrons more reduced than the Ni–A and Ni–B states (Fig. 2), and the density of the bridging ligand "X", present in the A and B states, has disappeared in the electron density map of the x-ray data of reduced crystals [4,7]. The Ni–C state is characterized by *g* values of 2.01, 2.15, and 2.20 (see, e.g., for *D. vulgaris* Miyazaki F hydrogenase [51]). Similar to the Ni–A and Ni–B states, such a set of *g* values, with one being close to the free electron *g* value, g_e, and two shifted from g_e, indicate that the unpaired electron occupies the $3d_{z^2}$ orbital of nickel and that the nickel is most probably five-coordinated. The single crystal EPR studies [51] indeed showed that the direction of the principal *z* axis of the **g** tensor is oriented similar to Ni–A and Ni–B, i.e., parallel to the bond direction from nickel to the sulfur of the axial cysteine, and pointing from nickel to the vacant axial coordination position (see Fig. 7). This also indicates that the bridging position "X," one of the equatorial ligation positions of nickel, is still occupied (see Fig. 1). Since no significant electron density was observed in x-ray crystallography, this ligand must therefore be a light atom (or atoms).

In relation to the formal oxidation state, the Ni–C state was first expected to be an Ni^{I} (d^9) species. This is, however, not in line with XAS studies that show no significant change of the valence state [38], upon comparing Ni–A/Ni–B to Ni–C. The EPR parameters indicate the presence of a d_{z^2} ground state as found for Ni–A/Ni–B. A careful analysis of the single-crystal EPR data together with DFT calculations on various models of Ni–C incorporating different bridging ligands, indeed showed that this state is best described by a formal Ni^{III} d_{z^2} ground state, accommodating a hydride (H^-) in the bridge between Ni and Fe [51].

3.3. The Split Ni–C Signal

In general it is difficult to study the Ni–C state by EPR at low temperatures (<40 K). The reason for this is that the proximal [4Fe4S] cluster is usually also

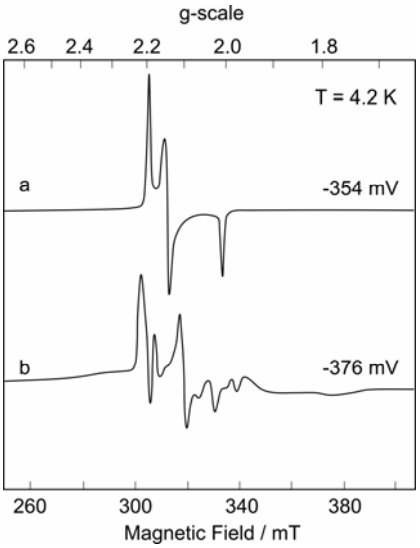

Figure 8. EPR spectra of (a) "unsplit" and (b) "split" Ni–C signal for *D. gigas* [NiFe] hydrogenase. The redox potential for (a) was set to –354 mV, for (b) to –376 mV. Experimental conditions: temperature, 4.2 K; microwave frequency, 9.378 GHz; microwave power, 0.01 mW (a) and 1 mW (b); modulation frequency, 100 kHz; modulation amplitude, 1 mT. Reproduced with permission from [53]. Copyright © 1995, American Chemical Society.

reduced and paramagnetic ($S = 1/2$). The spin–spin interaction between the [NiFe] center and the proximal $[4Fe4S]^+$ cluster splits and broadens the EPR spectrum [35,52,53]. Above this temperature, the electronic relaxation time of the $[4Fe4S]^+$ cluster is so fast that the spin–spin interaction is averaged out. An exception is the regulatory hydrogenase of *R. eutropha*, which has midpoint potentials such that the proximal [4Fe4S] cluster remains oxidized ($S = 0$), when the [NiFe] center is in the Ni–C state, and no spin–spin interaction is observed at low temperatures.

The midpoint potentials for *D. gigas* hydrogenase, at pH 7.0, –270 mV for the appearance and –390 mV for the disappearance of the Ni–C signal, are strongly pH dependent [34]. From the amount of "split" and "unsplit" Ni–C state present in the EPR spectrum at low temperature, the midpoint potential of the [4Fe4S] cluster was estimated to be –350 mV (–60 mV/pH unit) [34]. It is therefore possible to carefully set the potential to obtain a maximum amount of "unsplit" Ni–C signal at low temperatures, so that pulsed ENDOR and ESEEM experiments on Ni–C can be recorded [54]. Since these potentials are close together and vary between species, it may not always be possible to obtain unsplit Ni–C signals.

The splitting of the EPR spectrum at low temperature can advantageously be used to measure the spin–spin interaction between the [NiFe] center and the reduced proximal $[4Fe4S]^+$ cluster. This has been done by Guigliarelli et al. using multifrequency EPR [52] (see Fig. 8). It was found that the spin–spin interaction

observed in EPR is restricted to that between the [NiFe] center and the proximal $[4Fe4S]^+$ cluster; the J coupling constant that leads to the best simultaneous fit of the multifrequency EPR spectra is 40×10^{-4} cm^{-1} [52,53]. In addition, the relative orientations of the **g** tensors of the [NiFe] center and the [4Fe4S] cluster in terms of three Euler angles have been elucidated from simulations.

From such measurements information about the identity, coupling strength, distance, and even relative orientation of other paramagnetic centers in the enzyme can, in principle, be obtained. This is of utmost importance for understanding the electron transfer between the metal centers in the enzyme. In this respect, more information is still required for understanding the exact electron transfer pathway in the hydrogenases.

3.4. The Light-Induced State Ni–L

In contrast to the Ni–A and Ni–B redox states, the EPR spectrum of the Ni–C state changes when the sample is illuminated with white light at low temperatures (<180 K) [34,55]. Up to three light-induced states have been identified for [NiFe] hydrogenases [35,56], depending on the temperature at which the illumination was performed, the duration of the illumination, and the source of the enzyme. The light-induced states are commonly referred to as Ni–L1, Ni–L2, and Ni–L3, all of which have different g values. The Ni–L states can be annealed back to Ni–C when the temperature is raised, which shows that the photoprocess is fully reversible. For *T. roseopersicina* hydrogenase, the temperature dependence was investigated by EPR spectroscopy, and a recovery to Ni–C upon annealing was observed at temperatures above ~180 K [57]. The g values of the Ni–L states vary slightly depending on the origin of the enzyme. For *D. gigas* hydrogenase, they are 2.264, 2.113, and 2.044 for Ni–L1, 2.293, 2.124, and 2.045 for Ni–L2, and 2.41 and 2.16 for Ni–L3 (the lowest g value could not be determined for Ni–L3). The values are very similar for *D. vulgaris* Miyazaki F, for which only 2 states were observed (see Table 1) [58]. Compared to Ni–C, the largest g value of the Ni–L states is increased, and also the smallest g value has become larger (typically 2.05). The latter change suggests that the Ni–L states can no longer be described as pure $3d_{z^2}$ ground states [46], since for such states ligand field theory indicates that the smallest g value is equal or very close to $g_e = 2.0023$.

The observation of a g_z value significantly larger than g_e has prompted researchers to suggest that the Ni–L states are formal Ni^I $3d^9$ states, in which the unpaired electron resides in the $3d_{x^2-y^2}$ orbital [59,60]. XAS data, however, indicate that the nickel in Ni–L is slightly more reduced than in Ni–C, but the observed edge shift is too small to justify a description as an Ni^I state [41]. The single-crystal EPR data of Ni–L show that the orientation of the g_z principal axis is still parallel to the bond direction from nickel to the axial cysteine (or to the free coordination position) [51], indicating that the wavefunction of the unpaired electron is still dominated by the $3d_{z^2}$ orbital on nickel. Indeed, ligand field considerations show that only a small admixture of the $3d_{x^2-y^2}$ to the $3d_{z^2}$ orbital is sufficient to shift the g_z value from 2.01 to 2.05 [46]. This situation may be compared to the admixture of

some $3d_{z^2}$ orbital to the $3d_{x^2-y^2}$ ground state in blue copper proteins [61], which introduces a large rhombictiy in the *g* values. Whether the Ni–L states can formally be described as Ni^{I} or Ni^{III} d_{z^2} states is not clear at present. This depends critically on the relative energies of $d_{x^2-y^2}$ and d_{z^2}, and on the ligand orbitals.

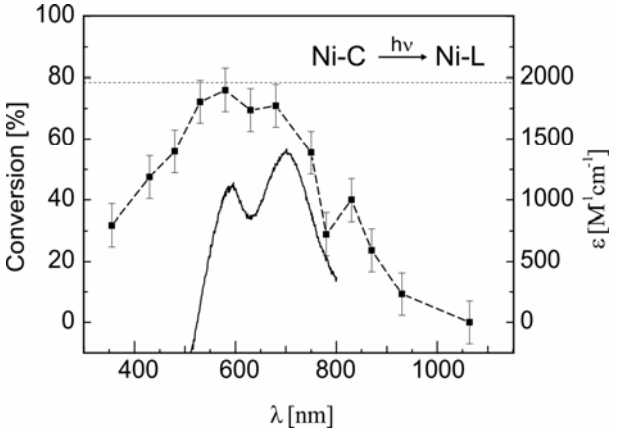

Figure 9. Conversion of Ni–C to Ni–L as derived from EPR decay curves (Ni–C signal decay at $g_x = 2.20$) at different wavelengths of the excitation light (dashed line). Also included is the UV/VIS spectrum of the reduced enzyme (500–800 nm). For further details see [62]. Reproduced with permission [62]. Copyright © 2003, Royal Society of Chemistry.

The action spectrum associated with Ni–C → Ni–L2 conversion has recently been investigated by EPR spectroscopy for *D. vulgaris* Miyazaki F [62], and it is illustrated in Figure 9. It turned out that the action spectrum is broad and spans the complete visible range. Nevertheless, some structure was observed with local maxima at 590, 700, and 850 nm. The wavelengths of the first two maxima correspond to those observed in the UV/VIS spectrum of the reduced enzyme, indicating that the conversion process may be a direct process in which the light is absorbed by the [NiFe] center itself. However, based on the available data [62], an additional mechanism according to which the light is absorbed by the nearby [4Fe4S] cluster and the energy is transferred to the [NiFe] center cannot be excluded.

3.5. The Ni–CO State

The [NiFe] hydrogenases are inhibited by CO. Recent x-ray data show that the CO binds at the 6th coordination position (opposite to the axial sulfur) and that it is photolabile [8]. Binding of CO causes a change in the electronic structure and the EPR *g*-values (2.12, 2.07, 2.02). Addition of ^{13}CO [36] results in a large, almost isotropic ^{13}C HFC of 85 MHz. Initially, it was proposed that Ni–C binds the CO. Later work [19] suggested that Ni–L might attach the CO. Best agreement between experimental data and DFT calculations was obtained when the CO is bound to Ni as a π electron acceptor, for which the calculations yield *g* values of 2.11, 2.06, and

2.00 and a ^{13}C HFC of 72 MHz [63]. So far, a single-crystal EPR study of the Ni–CO state has not been reported.

4. ENDOR AND ESEEM STUDIES OF [NIFE] HYDROGENASE: HYPERFINE STRUCTURE

In this section, hyperfine coupling constants (HFCs) observed by hyperfine resolving techniques such as ENDOR or ESEEM/HYSCORE are discussed. The advantage of these techniques lies in direct determination of the hyperfine coupling parameters, which give information about the spin density distribution over the metal centers and the ligand sphere. Additionally, when applied to single crystals, the techniques also allow elucidation of the principal axes of the hyperfine tensor, which can advantageously be used to determine bond directions or orientations of small molecules bound to or near the active site.

Several specific problems have been addressed using hyperfine spectroscopy on the [NiFe] hydrogenases:

1. Measurement of the HFCs of the metal nuclei by the use of isotopically labeled (^{61}Ni, ^{57}Fe) hydrogenase.
2. Magnitudes of HFCs of ligand nuclei to estimate the spin density distribution.
3. Identification of bridging ligand X by determination of the respective hyperfine data using labeling and exchange procedures.
4. Light sensitivity of Ni–C.
5. Interaction with the protein surrounding.

4.1. Hyperfine Couplings of Metal Nuclei

A question of major importance for the electronic structure of the active center is the spin density distribution over the heterobimetallic [NiFe] center. A direct approach is provided by measuring the spin density at the nickel and at the iron in the paramagnetic states of the enzyme. This has become possible by labeling the enzyme with ^{61}Ni ($I = 3/2$) and ^{57}Fe ($I = 1/2$), respectively. ^{57}Fe ENDOR experiments have shown that the Fe contains a negligible amount of electron spin density in both oxidized states [64]. Similar experiments on the Ni–C state also showed a very small ^{57}Fe HFC (< 1 MHz) [64]. These experiments are in line with iron being in the low-spin Fe^{II} state ($S = 0$) in all redox states of the enzyme. The small amount of spin density at the iron is caused by spin polarization.

^{61}Ni labeling was already employed in early investigations to unambiguously identify the presence of nickel in this class of enzymes [65,66]. For the unready (Ni–A) state of *Methanobacterium thermoautotrophicum* hyperfine coupling constants of $A_x = 21.0$, $A_y = 42.0$, and $A_z = 75.9$ MHz have been elucidated from simulations of cw-EPR experiments [65]. More recently ^{61}Ni labeling of *D. vulgaris* Miyazaki F has been performed and the EPR analysis led to a set of ^{61}Ni HFCs for all paramagnetic states in this hydrogenase [58].

Calculation of the ^{61}Ni HFCs is difficult, in particular for the isotropic part [67]. The data reported recently using DFT [68] are, however, in satisfy-

ing agreement with the available experimental data. This is further evidence that the recent improvements in property calculations of DFT methods [67,69] allows one to reliably predict the observables related to electronic structure of the [NiFe] hydrogenase for small geometry optimized structural models (for details, see [49,63,68,70–81]).

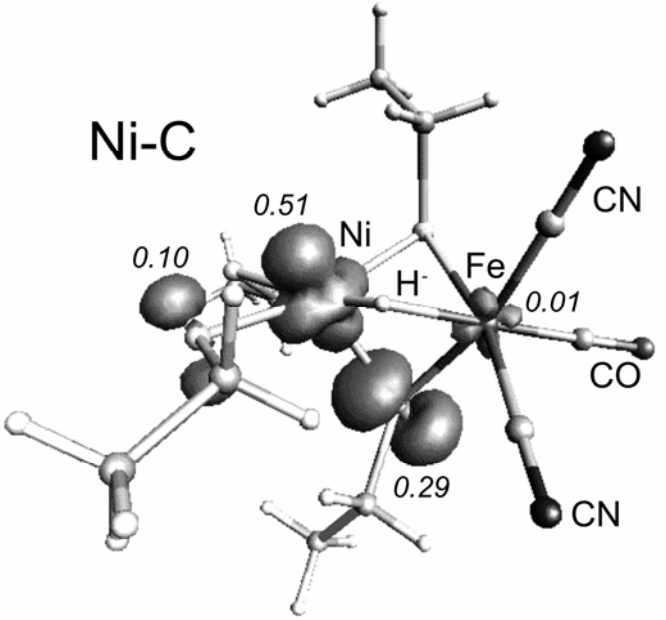

Figure 10. Contour plot of the unpaired spin density distribution ($0.005\ e/a_0^3$), DFT (BLYP/DZVP) of a truncated model of the active site in the Ni–C state (Ni^{III}, Fe^{II}, hydride bridge). The Mulliken atomic spin densities are given [76]. In the oxidized ready Ni–B state (OH^- bridge), the spin density at the Ni is almost the same (0.52), at the sulfurs (0.34 and 0.06, axial and equatorial) it is somewhat changed; at Fe and at the bridge it is vanishingly small. For other theoretical results, see [71,78] .

The data analysis shows that in the oxidized and the reduced states negligible spin density is found at the Fe. The nickel carries more than 50% of the spin. The remaining spin density is distributed over the (sulfur) ligands of the active site. This is supported by detection of a large ^{33}S HFC in the [NiFe] hydrogenase of *A. vinosum* [82] and also by the ^1H HFCs of the cysteines (see below). A model of the active site used in DFT calculations [76] is shown in Figure 10, depicting the calculated spin density distribution of the Ni–C state ($X = H^-$).

4.2. HFCs of Ligand Nuclei

Single-crystal ENDOR studies of the Ni–B state [83] showed two large non-exchangeable ^1H HFCs that could be assigned to the methylene (CH_2) protons of the bridging cysteine axially coordinated to the nickel (Fig. 1). This is in agreement

with earlier ENDOR studies of Ni–B in frozen solutions of *A. vinosum* [84]. The two signals associated with the couplings (A1 = [17.0, 11.4, 10.9] MHz, A2 = [13.4, 10.1, 10.1] MHz) are shown in Figure 11. This finding is in line with the presence of significant spin density at the axial cysteine sulfur. Couplings of similar magnitude are found for Ni–A, [85], and Ni–C [86]. This strongly supports the model of a Ni^{III} d_{z^2} ground state with the spin-carrying orbital oriented along an axis pointing toward this sulfur atom. DFT calculations indicate a spin density of up to ~30% at the respective sulfur (Fig. 10); a small amount of spin density is also found at one of the equatorial cysteine sulfur atoms.

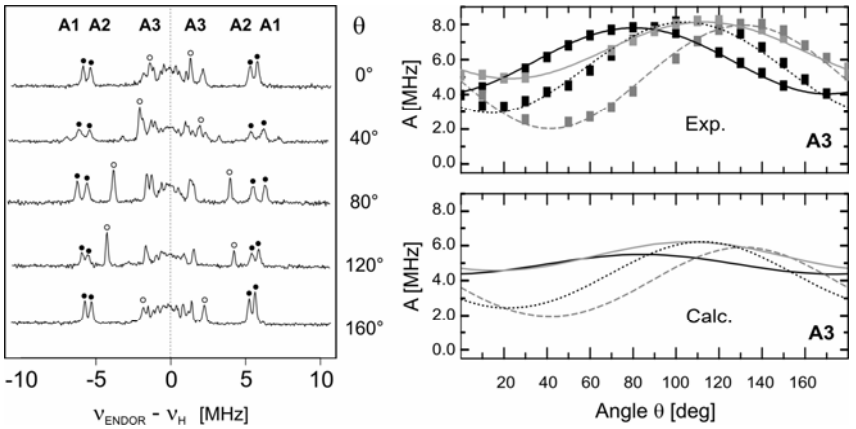

Figure 11. *Left:* Pulse ENDOR spectra for one site of Ni–B in a single crystal of [NiFe] hydrogenase of *D. vulgaris* Miyazaki F (selected traces). The 3 major hyperfine splittings (A1, A2, A3) are indicated by dots. *Right:* angular dependence of the HFC of the exchangeable proton A3 for the four sites in the single crystal (cf. Fig. 6). In the lower panel the orientation dependence of the respective proton HFC obtained from a DFT calculation is shown. Although the absolute magnitude of the HFC is somewhat smaller, the angular dependence is in perfect agreement with the experiment. Based on this comparison, the ^{1}H HFC has been assigned to the OH^{-} ligand bridging the Ni and the Fe. The respective proton is located close to the plane of the Ni d_{z^2} orbital. For further details, see [83].

4.3. The Bridging Ligand X

Since it is known that the identity of the 3rd bridging ligand is changed upon activation of the enzyme and also in the catalytic cycle, its clear identification in the different states is of utmost importance. This can be achieved by EPR/ENDOR techniques.

4.3.1. Ni–A/Ni–B

Isotope labeling experiments, using molecular $^{17}O_2$ for both Ni–A and Ni–B [36], and also $H_2{}^{17}O$ for Ni–A ($A(^{17}O)$ = [5, 7, 20] MHz) [87] showed that the

bridging ligand in both states contains an oxygen atom. In the latter study, it was shown that exchange of the bridge to a ^{17}O-labeled one is only possible if a reduction–oxidation cycle is performed, demonstrating the relative inaccessibility of the [NiFe] center in the Ni–A state as compared to the Ni–B state.

The presence of a sulfur species (S^{2-}, SH^-, H_2S) in the bridge between Ni and Fe has been discussed by various authors [6,7,9,21,88]. For the Ni–A and Ni–B states (Fig. 5) this can, however, be excluded based on the ^{17}O data. It is expected that a sulfur-based ligand would lead to an EPR spectrum with different *g* values. Such minority species with different *g* values have recently been reported for the oxidized states of *D. vulgaris* Miyazaki F (see, e.g., Fig. 5 and [9,88]). However, up to now the identity of these species remains unclear.

For Ni–A, ENDOR experiments by Fan et al. in combination with deuterium exchange indicated that no exchangeable proton near the [NiFe] center is present [89]. Also with ESEEM, no exchangeable proton has been observed [90]. For Ni–B, the [NiFe] center does have an exchangeable proton, as was found for the enzyme of *A. vinosum* by careful measurement of the g_z signal and examination of the superhyperfine structure [91]. Recently it has been shown that for Ni–A it is also possible to exchange a proton near the active site, by first exchanging the solvent to D_2O, followed by reduction with D_2 gas to remove the bridging ligand and reoxidation to restore an isotopically labeled bridge. With this reduction–reoxidation treatment, a deuterium signal could be observed in ESEEM and HYSCORE spectroscopy for Ni–A [80] and an HFC could be estimated. This was fully corroborated by recent single-crystal ENDOR experiments of Ni–A (Ogata et al., unpublished data).

Single-crystal ENDOR experiments of the Ni–B state have been used to elucidate the complete HFC tensor of the proton of the bridging ligand (principal values are [−8.2, −7.0, +3.6] MHz) [83] (see Fig. 11). Early DFT calculations suggested the presence of an OH^- bridge for Ni–B [63,77,92]. By comparison with DFT calculations of the hyperfine tensors in a model of the active site, it was found that Ni–B contains an OH^- bridge and that two possible binding modes for an OH^- exist, and one of them could be favored based on a comparison between experimental and DFT data [83] (see Fig. 11). For the Ni–A state an experimental verification of the identity of the bridging ligand is not yet available. Possible candidates are OH^-, bound in a different conformation, H_2O, or OOH^- [83].

4.3.2. Ni–C

In the Ni–C state, pioneering ENDOR experiments in the groups of Hoffman and Moura have shown for *D. gigas* hydrogenase that a proton with a very large hyperfine coupling constant (a_{eff} = 16.8 MHz) is present, which seems to interact directly with the nickel [89]. This proton was found to be exchangeable, and one of the proposed assignments was that it could belong to an in-plane (i.e., equatorial) hydrogen directly bonded to nickel (e.g., a hydride). This would favor a formal Ni^{III} redox state for Ni–C [89]. A second exchangeable proton with $a_{eff} \approx 4.4$ MHz was also observed in this work.

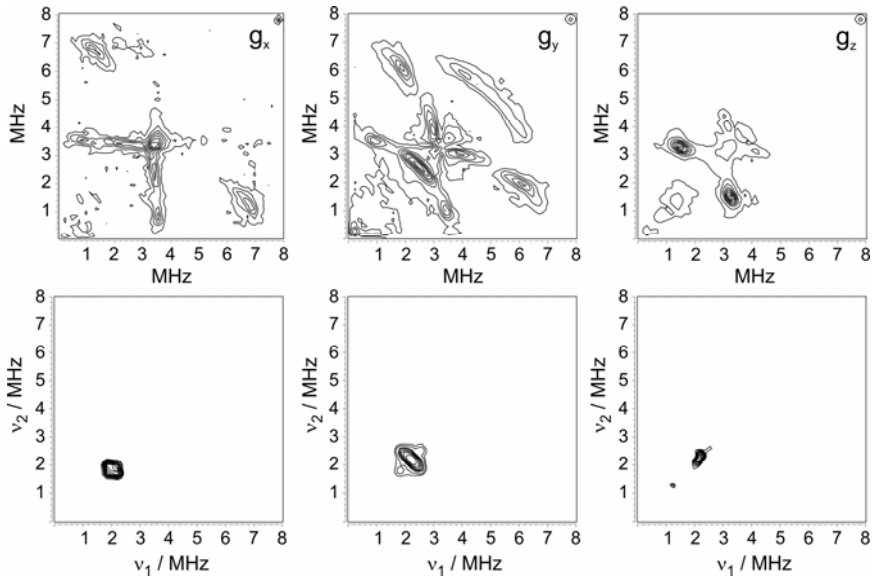

Figure 12. ^{2}H HYSCORE spectra taken along g_x, g_y, and g_z of the Ni–C and Ni–L1 states of the regulatory hydrogenase of *R. eutropha* in D_2O buffer. The large deuterium coupling of the exchangeable proton (deuteron) observed for Ni–C collapses to a structureless band at the ^{2}H Larmor frequency (close to 2 MHz), demonstrating the photodissociation of the hydride upon illumination at $T = 77$ K in the Ni–C $\rightarrow$ Ni–L1 transition [93]. The process is fully reversible.

In a recent study of the Ni–C state in the RH of *R. eutropha* [23] and in *D. vulgaris* Miyazaki F [86] using orientational selection ENDOR and HYSCORE in combination with H/D exchange, the complete HFC tensor of the exchangeable proton could be determined (principal values are [+21.9, −7.3, −14.5] MHz). The data are only compatible with the presence of a hydrogen in the bridge between Ni and Fe, bound in the equatorial plane of the metal. The obtained tensor is in good agreement with DFT calculations. Illumination of Ni–C removes the signals related to this proton from the spectrum (see Fig. 12). By using the results from the **g** tensor analysis in Ni–C [51], this proton is assigned to the hydride in the bridging position, which is derived from the heterolytic splitting of the substrate hydrogen. In these contributions [51,86] a key intermediate in the hydrogenase catalytic cycle has been structurally characterized.

4.4. Light Sensitivity of the Active Intermediate

Illumination of the Ni–C state of all hydrogenases at low temperatures creates a light-induced state (Ni–L) with a significantly different EPR spectrum. Different forms of these species have been reported (Table 1).

In the Ni–L state the large ^{1}H HFC of the H^- bridge in Ni–C observed by ENDOR and HYSCORE spectroscopy vanishes [23,57,86,89] (see Fig. 12). After annealing of the sample, the Ni–C EPR signal and the large hyperfine interaction is recovered. This observation strongly indicates that the photoconversion of Ni–C to the Ni–L states involves a photodissociation of the bound hydride. With deuterium exchange experiments it was shown that the rich structure in the ^{2}H region of the HYSCORE spectrum of Ni–C (see Fig. 12) collapses into an unstructured band at the ^{2}H Larmor frequency [23] for Ni–L. However, signals could still be observed, indicating that upon photodissociation the proton remains in the close vicinity of the center. Since up to three different Ni–L states are observed that are very similar with respect to their spectroscopic properties, it is tempting to speculate that the three equatorial cysteine residues may act as bases and take up the proton. However, at present no experimental data exist to validate this hypothesis. A detailed ENDOR study of the Ni–L states is still lacking [93].

4.5. Interaction of the Active Site with the Protein Surrounding

The [NiFe] center of the hydrogenase is bound to the protein via 4 cysteines, as shown in Figure 1. However, further non-covalent interactions have been identified for this site [3]. The latter include hydrogen bonds to the sulfur and CN^- groups and also hydrophilic and electrostatic interactions. In all catalytic [NiFe] hydrogenases a highly conserved histidine residue is present, which is in a position to form an H-bond to the axial cysteine sulfur with respect to Ni (Fig. 1).

It is interesting to note that 3-pulse ESEEM and HYSCORE spectra of both Ni–A [90] and Ni–B [81] indicated the presence of a nitrogen atom. Since nitrogen is not found in the first ligand sphere of the [NiFe] center, it can only belong to a more remote amino acid ligand, which still interacts with the paramagnetic site. By inspection of the x-ray structure, and determination of the complete hyperfine and quadrupole tensor for ^{14}N (I = 1), the nitrogen could be identified as an imidazole (N–H) nitrogen. Moreover, the N–H fragment of the imidazole forms a hydrogen bond to the axial sulfur, which carries a significant amount of electron spin density [81]. The respective histidine ligand is highly conserved in all catalytically active [NiFe] hydrogenases. It is, however, absent in the regulatory hydrogenase of *R. eutropha* [22], where indeed no nitrogen modulations were observed in the ESEEM spectra. It has been discussed that the hydrogen-bonded histidine plays a role in fine tuning the electronic properties of the active site and might therefore have a functional role [81]. The latter point became clear in the Q67H mutant of *R. eutropha* hydrogenase, in which a histidine was introduced in the homologous position of the standard hydrogenases [22]. This mutant showed very similar ESEEM spectra to the standard hydrogenase, indicating that the hydrogen bond had been established in the mutant.

5. DISTANCE STUDIES OF [NIFE] HYDROGENASES

The size of the spin–spin interaction of the [NiFe] center and the [3Fe4S] cluster ($S = ½$) is within the range that can be studied by pulse ELDOR spectroscopy. This PELDOR technique allows measurement of the spin–spin interaction and a determination of the effective distance between the two electron spins. Measurements have so far only been performed for *D. vulgaris* Miyazaki F hydrogenase [94] on the as-isolated enzyme (30% Ni–A and 70% Ni–B). The spin delocalization over the [3Fe4S] cluster had to be included for correct data analysis. Spin projection coefficients have been determined that indicate that the largest amount of electron spin density is located on the iron closest to the [NiFe] center.

6. EPR-SILENT STATES

The intermediate states Ni–SU, Ni–SIr, Ni–SIa, and Ni–R, where the number of electrons in the [NiFe] center is even, are commonly denoted as EPR-silent states. X-ray absorption spectroscopy (XAS) experiments are compatible with a formal Ni^{II} in the EPR-silent states (Ni–SU; Ni–SI; Ni–R) [38,41]. With Ni L-edge XAS it was found that the Ni^{II} is most likely in a high-spin state ($S = 1$) [95]. This has so far not been corroborated by EPR spectroscopy, possibly because of the presence of a large zero-field splitting that makes it impossible to detect the signal at X-band frequencies (9 GHz).

The high-spin or low-spin character of the "EPR-silent" Ni^{II} states depends on the energy splitting of the $d_{x^2-y^2}$ and d_{z^2} orbitals (as shown in Fig. 3). When these orbitals are sufficiently close in energy, the high-spin ground state is favored in which each orbital carries one electron. The distortion, which most efficiently brings the $d_{x^2-y^2}$ orbital down in energy, is one toward a trigonal (bi)pyramid [44]. Whether or not the orbitals come close enough to yield the high spin state as the ground state is a question that may have to be addressed by high-field EPR, by which paramagnetic states with a large zero-field splitting can be observed. The possibility to observe the Ni^{II} high-spin states will depend on the magnitude of the zero-field splitting. For a typical value of 3 cm^{-1}, an instrument working at 90 GHz or higher is required.

7. CONCLUSIONS AND OUTLOOK

Based on the single-crystal EPR data collected for the paramagnetic states of the [NiFe] hydrogenase it can be concluded that Ni–A, Ni–B, Ni–C are formally Ni^{III} d^7 species with a $d^1_{z^2}$ ground state ($S = 1/2$). The nickel ion has a square pyramidal coordination geometry, and it is believed that the substrate hydrogen (initially) binds to the sixth (free) coordination position at the Ni. The light-induced Ni–L states have a mixed $d_{z^2} / d_{x^2-y^2}$ ground state. According to crystal field theory, the Ni in Ni–L is in a formal d^9 Ni^{I} state. However, the sulfur ligands may lead to strong delocalization of the electrons and a more positive charge at Ni. The iron in the [NiFe] hydrogenase has an octahedral coordination geometry; it is in a d^6 Fe^{II} low-spin state and thus diamagnetic ($S = 0$). This is probably caused by the strong inorganic CO and CN^- ligands attached to the iron site.

The additional third bridging ligand X between Ni and Fe seems to play an important role for the hydrogenase since it changes its identity in the functional cycle. In the oxidized states this bridging position is occupied by an oxygenic species. For the ready state Ni–B this is a μ-hydroxo (OH^-) [83], while in the unready state Ni–A a final identification has not been achieved. In the activation process of the enzyme the bridging ligand (e.g., OH^- in Ni–B) must be removed. A possible mechanism involves protonation of the OH^- (Ni–B) and subsequent release as water [68], leading to a highly active species (Ni–SIa) that is EPR silent (cf. Fig. 2) [14].

A key intermediate in the reaction cycle is Ni–C, for which it was shown by EPR, ENDOR, and HYSCORE spectroscopy that it carries a μ-hydrido (H^-) bridge between Ni and Fe [23,51,86]. This is most probably directly derived from the substrate hydrogen. In a last reduction step the Ni–R state is reached, which is again EPR silent. The enzyme shuttles between the Ni^{III} (EPR-active) and Ni^{II} (EPR-silent) states in the catalytic cycle (Fig. 2).

Heterolytic H_2 dissociation must occur before the formation of Ni–C in the EPR-silent NiSI states. Mechanistic models for this process have recently been discussed [14,68,79,96]. The paramagnetic light-induced Ni–L states derived from Ni–C have lost the hydride bridge [23,86]. The released proton is attached to a nearby base, possibly one of the sulfurs of the cysteine ligands. The Ni–C to Ni–L conversion process is reversible. The CO-inhibited paramagnetic state Ni–CO is probably derived from the Ni–L state. The CO ligand is attached to the nickel and blocks hydrogen access [8,19]. A similar situation is likely to occur when the enzyme is inhibited by O_2 [9,96]. However, in the case of oxygen additional structural and electronic changes at the cysteines of the enzyme seem to occur as well [5,9].

The EPR studies on the paramagnetic states [98]—together with other investigations using, for example, FTIR and XAS studies that can be applied to the EPR-silent states—have delivered important insight into the catalytic cycle of [NiFe] hydrogenase as well as in activation/deactivation and inhibition of this important enzyme. However, the picture is still far from being complete.

Open questions remain concerning the identity of the bridging ligand in Ni–A. This is important for understanding oxygen sensitivity and inhibition of this enzyme. With the information that the bridging ligand contains oxygen and a proton for both the Ni–A and Ni–B states, likely candidates for the bridge are OH^- and H_2O. However, recent x-ray crystallographic studies on single crystals in the Ni–A state indicate the presence of a bridging ligand, which could be OOH^- [5,9]. The two structures, available for the hydrogenases of *D. fructosovorans* and *D. vulgaris* Miyazaki F, also contain modified cysteines (modeled as oxidized cysteines with an additional oxygen attached to sulfur). Different cysteines were found to be modified in the two structures. Furthermore, it has been discussed that sulfur species (HS^-, S^{2-}, H_2S) might occupy the bridging position in these bacteria [6,7,9,21]. However, a sulfur bridge would probably lead to an [NiFe] center with different EPR characteristics (*g* values).

It is also unclear what exactly happens to the hydride after it is photodissociated from the [NiFe] center and which amino acid is used as a base in the light-induced Ni–L states. Further studies on Ni–CO structures will provide insight into the mechanism of the catalytic cycle, as CO can inhibit the enzyme only after it has been reduced. The valence of the Ni–CO state is ambiguous, and investigation of the photolability of CO resulting in the same Ni–L structure as that obtained from Ni–C will contribute to understanding the electronic structure of the Ni–L states. Furthermore, the spin multiplicity of the "EPR silent" states is still not known. Though an EPR signal has not been reported, XAS measurements seem to favor a high-spin ground state [95].

The solution of these problems is crucial for formulation of a detailed reliable reaction mechanism that is based on experimental data. More information is also required concerning the H^+ and e^- transfer to the active site of the enzyme and also the H_2 channel (cf. Fig. 1). The influence of the protein surrounding on the structure, function, and dynamics of the hydrogenase has so far been little investigated. Very interesting would also be a comparison of the similarities and differences between the different classes of hydrogenases that use different active sites to convert hydrogen and show substantial differences in enzymatic activity [97,98]. Knowledge of the reaction intermediates is an essential prerequisite for understanding hydrogenase function and for efficiently using this enzyme in future biotechnological processes or as blueprints for designing bioinspired artificial hydrogen catalysts for the production of hydrogen [97].

ACKNOWLEDGMENTS

We gratefully acknowledge Maria E. Pandelia for critically reading and Bärbel Plaschkies and Birgit Deckers for their help with writing the manuscript and for preparing the figures. The authors also want to thank all coworkers who contributed to the results presented in this work and who are named in the respective references. Financial support was provided by the Max Planck Society and the EU (Contract No 516510 (NEST, SOLAR-H)).

REFERENCES

1. Vignais PM, Billoud B, Meyer J. 2001. Classification and phylogeny of hydrogenases. *FEMS Microbiol Rev* **25**:455–501.
2. Volbeda A, Charon M-H, Hatchikian EC, Frey M, Fontecilla-Camps JC. 1995. Crystal structure of the nickel-iron hydrogenase from *Desulfovibrio gigas*. *Nature* **373**:580–587.
3. Volbeda A, Garcin E, Piras C, De Lacey AL, Fernandez VM, Hatchikian EC, Frey M, Fontecilla-Camps JC. 1996. Structure of the [NiFe] hydrogenase active site: evidence for biologically uncommon Fe ligands. *J Am Chem Soc* **118**:12989–12996.
4. Garcin E, Vernede X, Hatchikian EC, Volbeda A, Frey M, Fontecilla-Camps JC. 1999. The crystal structure of a reduced [NiFeSe] hydrogenase provides an image of the activated catalytic center. *Structure* **7**:557–566.
5. Volbeda A, Martin L, Cavazza C, Matho M, Faber BW, Roseboom W, Albracht SPJ, Garcin E, Rousset M, Fontecilla-Camps JC. 2005. Structural difference between the

ready and unready oxidized states of [NiFe] hydrogenases. *J Biol Inorg Chem* **10**:239–249.
6. Higuchi Y, Yagi T, Yasuoka N. 1997. Unusual ligand structure in Ni–Fe active center and an additional Mg site in hydrogenase revealed by high resolution x-ray structure analysis. *Structure* **5**:1671–1680.
7. Higuchi Y, Ogata H, Miki K, Yasuoka N, Yagi T. 1999. Removal of the bridging ligand atom at the Ni-Fe active site of [NiFe] hydrogenase upon reduction with H_2, as revealed by X-ray structure analysis at 1.4 Å resolution. *Structure* **7**:549–556.
8. Ogata H, Mizogushi Y, Mizuno N, Miki K, Adachi S, Yasuoka N, Yagi T, Yamauchi O, Hirota S, Higuchi Y. 2002. Structural studies of the carbon monoxide complex of [NiFe]hydrogenase from *Desulfovibrio vulgaris* Miyazaki F: suggestion for the initial activation site for dihydrogen. *J Am Chem Soc* **124**:11628–11635.
9. Ogata H, Hirota S, Nakahara A, Komori H, Shibata N, Kato T, Kano K, Higuchi Y. 2005. Activation process of [NiFe] hydrogenase elucidated by high resultion x-ray analysis: conversion of the ready to unready state. *Structure* **13**:1635–1642.
10. Montet Y, Amara P, Volbeda A, Vernede X, Hatchikian EC, Field MJ, Frey M, Fontecilla-Camps JC. 1997. Gas access to the active site of Ni-Fe hydrogenases probed by X-ray crystallography and molecular dynamics. *Nat Struct Biol* **4**:523–526.
11. Matias PM, Soares CM, Saraiva LM, Coelho R, Morais J, LeGall J, Carrando MA. 2001. [NiFe] hydrogenase form *Desulfovibrio desulfuricans* ATCC 27774: gene sequencing, three-dimensional structure determination and refinement at 1.8 Å and modelling studies of its interaction with the tetrahaem cytochrome c_3. *J Biol Inorg Chem* **6**:63–81.
12. Bagley KA, Duin EC, Roseboom W, Albracht SPJ, Woodruff WH. 1995. Infrared-detectable groups sense changes in charge density on the nickel center in hydrogenase from *Chromatium vinosum*. *Biochemistry* **34**:5527–5535.
13. Bagley KA, van Garderen CJ, Chen M, Duin EC, Albracht SPJ, Woodruff WH. 1994. Infrared studies on the interaction of carbon monoxide with divalent nickel in hydrogenase from *Chromatium vinosum*. *Biochemistry* **33**:9229–9236.
14. Bleijlevens B, van Broekhuizen F, De Lacey AL, Roseboom W, Fernandez VM, Albracht SPJ. 2004. The activation of the [NiFe]-hydrogenase from *Allochromatium vinosum*: an infrared spectro-electrochemical study. *J Biol Inorg Chem* **9**:743–752.
15. Coremans JMCC, van Garderen CJ, Albracht SPJ. 1992. On the redox equilibrium between H_2 and hydrogenase. *Biochim Biophys Acta* **1119**:148–156.
16. Coremans JMCC, van der Zwaan JW, Albracht SPJ. 1992. Distinct redox behaviour of the prosthetic groups in ready and unready hydrogenase from *Chromatium vinosum*. *Biochim Biophys Acta* **1119**:157–168.
17. George S.J., Kurkin S., Thorneley RNF, Albracht SPJ. 2004. Reactions of H_2, CO, and O_2 with active [NiFe]-hydrogenase from *Allochromatium vinosum*: a stopped-flow infrared study. *Biochemistry* **43**:6808–6819.
18. Kurkin S., George S.J., Thorneley RNF, Albracht SPJ. 2004. Hydrogen-induced activation of the [NiFe]-hydrogenase from *Allochromatium vinosum* as studied by stopped-flow infrared spectroscopy. *Biochemistry* **43**:6820–6831.
19. Happe RP, Roseboom W, Albracht SPJ. 1999. Pre-steady-state kinetics of the reactions of [NiFe]-hydrogenase from *Chromatium vinosum* with H_2 and CO. *Eur J Biochem* **259**:602–608.
20. Roseboom W, De Lacey AL, Fernandez VM, Hatchikian EC, Albracht SPJ. 2006. The active site of the [FeFe]-hydrogenase from *Desulfovibrio desulfuricans*, II: redox prop-

erties, light sensitivity and CO-ligand exchange as observed via infrared spectroscopy. *J Biol Inorg Chem* **11**:102–118.
21. Bleijlevens B, Buhrke T, van der Linden E, Friedrich B, Albracht SPJ. 2004. The auxiliary protein HypX provides oxygen tolerance to the soluble [NiFe]-hydrogenase of *Ralstonia eutropha* H16 by way of a cyanide ligand to nickel. *J Biol Chem* **279**:46686–46691.
22. Buhrke T, Brecht M, Lubitz W, Friedrich B. 2002. The H_2 sensor of *Ralstonia eutropha*: biochemical and spectroscopic analysis of mutant proteins modified at a conserved glutamine residue close to the [NiFe] active site. *J Biol Inorg Chem* **7**:897–908.
23. Brecht M, van Gastel M, Buhrke T, Friedrich B, Lubitz W. 2003. Direct detection of a hydride ligand in the [NiFe] center of the regulatory hydrogenase from *Ralstonia eutropha* in its reduced state by HYSCORE and ENDOR spectroscopy. *J Am Chem Soc* **125**:13075–13083.
24. Happe RP, Roseboom W, Egert G, Friedrich CG, Massanz C, Friedrich B, Albracht SPJ. 2000. Unusual FTIR and EPR properties of the H_2-activating site of the cytoplasmic NAD-reducing hydrogenase from *Ralstonia eutropha*. *FEBS Lett* **466**:259–263.
25. Kleihues L, Lenz O, Bernhard M, Buhrke T, Friedrich B. 2000. The H_2 sensor of *Ralstonia eutropha* is a member of the subclass of regulatory [NiFe] hydrogenase. *J Bacteriol* **182**:2716–2724.
26. Löscher S, Burgdorf T, Buhrke T, Friedrich B, Dau H, Haumann M. 2005. Non–standard structures of the Ni-Fe cofactor in the regulatory and the NAD-reducing hydrogenases from *Ralstonia eutropha*. *Biochem Soc Trans* **33**:25–27.
27. Pierik AJ, Schmelz M, Lenz O, Friedrich B, Albracht SPJ. 1998. Characterization of the active site of a hydrogen sensor from *Alcaligenes eutrophus*. *FEBS Lett* **438**:231–235.
28. van der Linden E, Faber BW, Bleijlevens B, Burgdorf T, Bernhard M, Friedrich B, Albracht SPJ. 2004. Selective release and function of one of the two FMN groups in the cytoplasmic NAD^+-reducing [NiFe]-hydrogenase from *Ralstonia eutropha*. *Eur J Biochem* **271**:801–808.
29. Lenz O, Friedrich B. 1998. A novel multicomponent regulatory system mediates H_2 sensing in *Alcaligenes eutrophus*. *Proc Natl Acad Sci USA* **95**:12474–12479.
30. Happe RP, Roseboom W, Pierik AJ, Albracht SPJ, Bagley KA. 1997. Biological activation of hydrogen. *Nature* **385**:126–126.
31. Frey M, Fontecilla-Camps JC, Volbeda A. 2001. Nickel–iron hydrogenases. In *Handbook of metalloproteins*, Vol. 2, pp. 880–896. Ed A Messerschmidt, R Huber, T Poulos, K Wieghardt. Chichester: John Wiley & Sons.
32. Volbeda A, Fontecilla-Camps JC. 2005. Structure–function relationship of nickel–iron sites in hydrogenase and a comparison with the active site of other nickel–iron enzymes. *Coord Chem Rev* **249**:1609–1619.
33. Fernandez VM, Hatchikian EC, Cammack R. 1985. Properties and reactivation of two different deactivated forms of *Desulfovibrio gigas* hydrogenase. *Biochim Biophys Acta* **832**:69–79.
34. Cammack R, Patil DS, Hatchikian EC, Fernandez VM. 1987. Nickel and iron–sulphur centres in *Desulfovibrio gigas* hydrogenase: ESR spectra, redox properties and interaction. *Biochim Biophys Acta* **912**:98–109.
35. Medina M, Williams R, Cammack R. 1994. Studies of light-induced nickel EPR signals in *Desulfovibrio gigas* hydrogenase. *J Chem Soc Faraday Trans* **90**:2921–2924.

36. van der Zwaan JW, Coremans JMCC, Bouwens ECM, Albracht SPJ. 1990. Effect of $^{17}O_2$ and ^{13}CO on EPR spectra of nickel in hydrogenase from *Chromatium vinosum*. *Biochim Biophys Acta* **1041**:101–110.
37. van der Zwaan JW, Albracht SPJ, Fontijn RD, Roelofs YBM. 1986. Electron-paramagnetic-resonance evidence for direct interaction of carbon-monoxide with nickel in hydrogenase from *Chromatium vinosum*. *Biochim Biophys Acta* **872**:208–215.
38. Gu Z, Dong J, Allan CB, Choudhury SB, Franco R, Moura JJG, Moura I, LeGall J, Przybyla AE, Roseboom W, Albracht SPJ, Axley MJ, Scott RA, Maroney MJ. 1996. Structure of the Ni site in hydrogenases by X-ray absorption spectroscopy: species variation and the effects of redox poise. *J Am Chem Soc* **118**:11155–11165.
39. Gu WW, Jacquamet L, Patil DS, Wang HX, Evans DJ, Smith MC, Millar M, Koch S, Eichhorn DM, Latimer M, Cramer SP. 2003. Refinement of the nickel site structure in *Desulfovibrio gigas* hydrogenase using range-extended EXAFS spectroscopy. *J Inorg Biochem* **93**:41–51.
40. Maroney MJ, Bryngelson PA. 2001. Spectroscopic and model studies of the Ni–Fe hydrogenase reaction mechanism. *J Biol Inorg Chem* **6**:453–459.
41. Davidson G, Choudhury SB, Gu Z, Bose K, Roseboom W, Albracht SPJ, Maroney MJ. 2000. Structural examination of the nickel site in *Chromatium vinosum* hydrogenase: redox state oscillation and structural changes accompanying reductive activation and CO binding. *Biochemistry* **39**:7468–7479.
42. De Lacey AL, Hatchikian EC, Volbeda A, Frey M, Fontecilla-Camps JC, Fernandez VM. 1997. Infrared-spectroelectrochemical characterization of the [NiFe] hydrogenase of *Desulfovibrio gigas*. *J Am Chem Soc* **119**:7181–7189.
43. Fichtner C, Laurich C, Bothe E, Lubitz W. 2006. Spectroelectrochemical characterization of the [NiFe] hydrogenase of *Desulfovibrio vulgaris* Miyazaki F. *Biochemistry* **45**:9706–9716.
44. Solomon EI, Pavel EG, Loeb KE, Campochiaro C. 1995. Magnetic circular-dichroism spectroscopy as a probe of the geometric of the geometric and electronic structure of nonheme ferrous enzymes. *Coord Chem Rev* **144**:369–460.
45. Abragam A, Bleaney B. 1970. *Electron paramagnetic resonance of transition ions*. Oxford: Clarendon Press.
46. Lubitz W, Brecht M, Foerster S, van Gastel M, Stein M. 2003. EPR and ENDOR studies of [NiFe] hydrogenase: contributions to understanding the mechanism of biological hydrogen conversion. *ACS Symp Ser* **858**:128–150.
47. LeGall J, Ljungdahl PO, Moura I, Peck HD, Xavier AV, Moura JJG, Teixeira M, Huynh BH, DerVartanian DV. 1982. The presence of redox-sensitive nickel in the periplasmic hydrogenase from *Desulfovibrio gigas*. *Biochem Biophys Res Comm* **106**:610–616.
48. Geßner C, Trofanchuk O, Kawagoe K, Higuchi Y, Yasuoka N, Lubitz W. 1996. Single crystal EPR study of the Ni center of NiFe hydrogenase. *Chem Phys Lett* **256**:518–524.
49. Cammack R, Patil DS, Aguirre R, Hatchikian EC. 1982. Redox properties of the ESR-detectable nickel in hydrogenase from *Desulfovibrio gigas*. *FEBS Lett* **142**:289–292.
50. Trofanchuk O, Stein M, Gessner Ch, Lendzian F, Higuchi Y, Lubitz W. 2000. Single crystal EPR studies of the oxidized active site of [NiFe] hydrogenase from *Desulfovibrio vulgaris* Miyazaki F. *J Biol Inorg Chem* **5**:36–44.
51. Foerster S, Stein M, Brecht M, Ogata H, Higuchi Y, Lubitz W. 2003. Single crystal EPR studies of the reduced active site of [NiFe] hydrogenase from *Desulfovibrio vulgaris* Miyazaki F. *J Am Chem Soc* **125**:83–93.

52. Guigliarelli B, More C, Fournel A, Asso M, Hatchikian EC, Williams R, Cammack R, Bertrand P. 1995. Structural organization of the Ni and the (4Fe–4S) centers in the active form of *Desulfovibrio gigas* hydrogenase: analysis of the magnetic interactions by electron paramagnetic resonance spectroscopy. *Biochemistry* **34**:4781–4790.
53. Dole F, Medina M, More C, Cammack R, Bertrand P, Guigliarelli B. 1996. Spin–Spin interactions between the Ni site and the [4Fe–4S] centers as a probe of light-induced structural changes in active *Desulfovibrio gigas* hydrogenase. *Biochemistry* **35**:16399–16406.
54. Müller A, Tscherny I, Kappl R, Hatchikian EC, Hüttermann J, Cammack R. 2002. Hydrogenase in the "active" state: determination of *g*-matrix axes and electron spin distribution at the active site by ^{1}H ENDOR spectroscopy. *J Biol Inorg Chem* **7**:177–194.
55. Cammack R, Fernandez VM, Schneider K. 1988. Nickel in hydrogenases from sulfate-reducing, photosynthetic, and hydrogen-oxidizing bacteria. In *The bioinorganic chemistry of nickel*, pp. 167–190. Ed CRD Lancaster. New York: VCH Publishers.
56. Medina M, Hatchikian EC, Cammack R. 1996. Studies of light-induced nickel EPR signals in hydrogenase: comparison of enzymes with and without selenium. *Biochim Biophys Acta* **1275**:227–236.
57. Whitehead JP, Gurbiel RJ, Bagyinka C, Hoffman BM, Maroney MJ. 1993. The hydrogen binding site in hydorgenase: 35-GHz ENDOR and XAS studies of the Ni–C active form and the Ni–L photoproduct. *J Am Chem Soc* **115**:5629–5635.
58. Foerster S. 2003. EPR spectroscopic investigation of the active site of [NiFe]-hydrogenase: a contribution to the elucidation of the reaction mechanism. PhD dissertation, Technische Universität Berlin.
59. van der Zwaan JW, Albracht SPJ, Fontijn RD, Slater EC. 1985. Monovalent nickel in hydrogenase from *Chromatium vinosum*. *FEBS Lett* **2**:271–277.
60. Sorgenfrei O, Klein A, Albracht SPJ. 1993. Influence of illumination on the electronic interaction between ^{77}Se and nickel in active F_{420}-non-reducing hydrogenase from *Methanococcus voltae*. *FEBS Lett* **332**:291–297.
61. Gewirth AA, Cohen SL, Schugar HJ, Solomon EI. 1987. Spectroscopic and theoretical studies of the unusual EPR parameters of distored tetrahedral cupric sites: correlations to X-ray spectral features of core levels. *Inorg Chem* **26**:1133–1146.
62. Fichtner C, van Gastel M, Lubitz W. 2003. Wavelength dependence of the photoinduced conversion of the Ni–C to the Ni–L redox state in the [NiFe] Hydrogenase of *Desulfovibrio vulgaris* Miyazaki F. *Phys Chem Chem Phys* **5**:5507–5513.
63. Stein M, Lubitz W. 2001. DFT calculations of the electronic structure of the paramagnetic states Ni–A, Ni–B and Ni–C of [NiFe] hydrogenase. *Phys Chem Chem Phys* **3**:2668–2675.
64. Huyett JE, Carepo M, Pamplona A, Franco R, Moura I, Moura JJG, Hoffman BM. 1997. ^{57}Fe Q-band pulsed ENDOR of the hetero-dinuclear site of nickel hydrogenase: comparison of the NiA, NiB, and NiC states. *J Am Chem Soc* **119**:9291–9292.
65. Albracht SPJ, Graf E-G, Thauer RK. 1982. The EPR properties of nickel in hydrogenase from *Methanobacterium thermoautotrophicum*. *FEBS Lett* **140**:311–313.
66. Moura JJG, Moura I, Huynh BH, Krüger H-J, Teixeira M, DuVarney RC, DerVartanian DV, Xavier AV, Peck Jr HD, LeGall J. 1982. Unambigous identification of the nickel EPR signal in ^{61}Ni-enriched *Desulfovibrio gigas* hydrogenase. *Biochem Biophys Res Comm* **108**:1388–1393.
67. Neese F. 2003. Metal and ligand hyperfine couplings in transition metal complexes: the effect of spin-orbit coupling as studied by coupled perturbed Kohn-Sham theory. *J Chem Phys* **118**:3939–3948.

68. Stein M, Lubitz W. 2004. Relativistic DFT calculations of the reaction cycle intermediates of [NiFe] hydrogenase: a model for the enzymatic mechanism. *J Inorg Biochem* **98**:862–877.
69. Neese F. 2001. Prediction of electron paramagnetic resonance g values using coupled perturbed Hartree-Fock and Kohn-Sham theory. *J Chem Phys* **115**:11080–11096.
70. Pavlov M, Siegbahn PEM, Blomberg MRA, Crabtree RH. 1998. Mechanism of H–H activation by nickel-iron hydrogenase. *J Am Chem Soc* **120**:548–555.
71. De Gioia L, Fantucci P, Guigliarelli B, Bertrand P. 1999. Ni–Fe hydrogenases: a density functional theory study of active site models. *Inorg Chem* **38**:2658–2662.
72. Pavlov M, Blomberg MRA, Siegbahn PEM. 1999. New aspects of H_2 activation by nickel–iron hydrogenase. *Int J Quantum Chem* **73**:197–207.
73. Stein M, van Lenthe E, Baerends EJ, Lubitz W. 2001. g- and A-tensor calculations in the zero-order approximation for relativistic effects of Ni complexes $(Ni(mnt)^{-}_2$ and $Ni(CO)_3H$ as model complexes for the active center of [NiFe]-hydrogenase. *J Phys Chem A* **105**:416–425.
74. Stein M, van Lenthe E, Baerends EJ, Lubitz W. 2001. Relativistic DFT calculations of the paramagnetic intermediates of the [NiFe] hydrogenase: implications for the enzymatic mechanism. *J Am Chem Soc* **123**:5839–5840.
75. Stein M, Lubitz W. 2001. The electronic structure of the catalytic intermediate Ni–C in [NiFe] and [NiFeSe] hydrogenases. *Phys Chem Chem Phys* **3**:5115–5120.
76. Stein M. 2001. Insight into the mechanism of [NiFe] hydrogenase by means of magnetic resonance experiments and DFT calculations. PhD dissertation, Technische Unversität, Berlin.
77. Stadler C, De Lacey AL, Montet Y, Volbeda A, Fontecilla-Camps JC, Conesa JC, Fernandez VM. 2002. Density functional calculations for modeling the active site of nickel-iron hydrogenases, 2: predictions for the unready and ready states and the corresponding activation processes. *Inorg Chem* **41**:4424–4434.
78. Amara P, Volbeda A, Fontecilla-Camps JC, Field MJ. 1999. A hybrid density functional theory/molecular mechanics study of nickel–iron hydrognease: investigation of the active site redox states. *J Am Chem Soc* **121**:4468–4477.
79. Bruschi M, Zampella G, Fantucci P, De Gioia L. 2005. DFT investigations of models related to the active site of [NiFe] and [Fe] hydrogenases. *Coord Chem Rev* **249**:1620–1640.
80. van Gastel M, Fichtner C, Neese F, Lubitz W. 2005. EPR experiments to elucidate the structure of the ready and unready states of the [NiFe] hydrogenase of *Desulfovibrio vulgaris* Miyazaki F. *Biochem Soc Trans* **33**:7–11.
81. Goenka Agrawal A, van Gastel M, Gärtner W, Lubitz W. 2006. Hydrogen-bonding affects the [NiFe] active site of *Desulfovibrio vulgaris* Miyazaki F hydrogenase: a hyperfine sublevel correlation spectroscopy and density functional theory study. *J Phys Chem B* **110**:8142–8150.
82. Albracht SPJ, Kröger A, van der Zwaan JW, Unden G, Böcher R, Mell H, Fontijn RD. 1986. Direct evidence for sulfur as a ligand to nickel in hydrogenase: an EPR study of the enzyme from *Wolinella-succinogenes* enriched in ^{33}S. *Biochim Biophys Acta* **874**:116–127.
83. van Gastel M, Stein M, Brecht M, Schröder O, Lendzian F, Bittl R, Ogata H, Higuchi Y, Lubitz W. 2006. A single-crystal ENDOR and density functional theory study of the oxidized states of the [NiFe] hydrogenase from *Desulfovibrio vulgaris* Miyazaki F. *J Biol Inorg Chem* **11**:41–51.

84. Geßner C, Stein M, Albracht SPJ, Lubitz W. 1999. Orientation-selected ENDOR of the active center in *Chromatium vinosum* [NiFe] hydrogenase in the oxidized "ready" state. *J Biol Inorg Chem* **4**:379–389.
85. Ogata H, et.al. 2006. unpublished data.
86. Foerster S, van Gastel M, Brecht M, Lubitz W. 2005. An orientation-selected ENDOR and HYSCORE study of the Ni–C active state of *Desulfovibrio vulgaris* Miyazaki F hydrogenase. *J Biol Inorg Chem* **10**:51–62.
87. Carepo M, Tierney DL, Brondino CD, Yang TC, Pamplona A, Telser J, Moura I, Moura JJG, Hoffman BM. 2002. ^{17}O ENDOR detection of a solvent-derived Ni–(OH_x)–Fe bridge that is lost upon activation of the Hydrogenase from *Desulfovibrio gigas*. *J Am Chem Soc* **124**:281–286.
88. Vincent KA, Belsey NA, Lubitz W, Armstrong FA. 2006. Rapid and reversible reactions of [NiFe] hydrogenases with sulfide. *J Am Chem Soc* **128**:7448–7449.
89. Fan C, Teixeira M, Moura JJG, Moura I, Huynh BH, LeGall J, Peck Jr HD, Hoffman BM. 1991. Detection and characterisation of exchangable protons bound to the hydrogen-activation nickel site of *desulfovibrio gigas* hydrogenase: a ^{1}H and ^{2}H Q-Band ENDOR study. *J Am Chem Soc* **113**:20–24.
90. Chapman A, Cammack R, Hatchikian EC, McCracken J, Peisach J. 1988. A pulsed EPR study of redox-dependent hyperfine interactions for nickel centre of *Desulfovibrio gigas* hydrogenase. *FEBS Lett* **242**:134–138.
91. Bleijlevens B, Faber BW, Albracht SPJ. 2001. The [NiFe] hydrogenase from *Allochromatium vinosum* studied in EPR-detectable states: H/D exchange experiments that yield new information about the structure of the active site. *J Biol Inorg Chem* **6**:763–769.
92. Stadler C, De Lacey AL, Hernandez B, Fernandez VM, Conesa JC. 2002. Density functional calculations for modeling the oxidized states of the active site of nickel-iron hydrogenases, 1: verification of the Method with Paramagnetic Ni and CO complexes. *Inorg Chem* **41**:4417–4423.
93. Brecht M. 2001. Hochfeld- und Puls-EPR-Untersuchungen an den Kofaktoren von [NiFe]-Hydrogenasen: Beiträge zur Klärung des Mechanismusses der biologischen Wasserspaltung. PhD dissertation, Technische Universität, Berlin.
94. Elsässer C, Brecht M, Bittl R. 2002. Pulsed electron-electron double resonance on multinuclear metal centers: assignement of spin projection factors based on the dipolar interaction. *J Am Chem Soc* **124**:12606–12611.
95. Wang H, Patil DS, Gu W, Jacquamet L, Friedrich S, Funk T, Cramer SP. 2001. L-edge X-ray absorption spectroscopy of some Ni enzymes: probe of Ni electronic structure. *J Elec Spec Rel Phen* **114–116**:855–863.
96. Lubitz W, van Gastel M, Gärtner W. 2007. Nickel iron hydrogenases. In *Metal ions in life sciences*. Ed A Sigel, H Sigel, RKO Sigel. Chichester: John Wiley & Sons. In press.
97. Morris RH. 2006. Hydrogenase and model complexes. In *Concepts and models in bioinorganic chemistry*, pp. 331–362. Ed H-B Kraatz, N Metzler-Nolte. Weinheim: Wiley-VCH.
98. Lubitz W, Reijerse E, van Gastel M. 2007. [NiFe] and [FeFe] hydrogenases studied by advanced magnetic resonance techniques. *Chem Rev* **107**:4331–4365.